Electrophoretic deposition of aluminum particles from pure propan-2-ol suspensions

Julien Wagner, Claudie Josse, Léa Gani, Stéphane Knittel, Pierre-Louis Taberna, Florence Ansart

Results in Materials 13 (2022) 100259

Contents lists available at ScienceDirect

Results in Materials

journal homepage: www.sciencedirect.com/journal/results-in-materials

Electrophoretic deposition of aluminum particles from pure propan-2-ol suspensions

Julien Wagner [a,b], Claudie Josse [c], Léa Gani [a], Stéphane Knittel [a], Pierre-Louis Taberna [b,*], Florence Ansart [b]

[a] Safran Aircraft Engines, Site Evry-Corbeil, France
[b] CIRIMAT, Université de Toulouse, CNRS, France
[c] UAR 3623 Centre de Microcaractérisation Raimond Castaing, France

ARTICLE INFO

Keywords:
Electrophoretic deposition process
Aluminum particles
Deposition parameters
Microstructure
Homogeneous coating

ABSTRACT

Aluminum (Al) coatings were deposited on 15CDV6 steel substrates using the electrophoretic deposition (EPD) process and pure propan-2-ol solvent. Key parameters in EPD process are the followings: solvent, additives, deposition conditions, electrical field, cell geometry. Herein, the influence of the applied electric field (0–60 Vcm^{-1}) and the deposition time (0–20 min) was precisely studied as a function of the deposition rate. A uniform and porous Al particle coating was targeted and obtained. Control of the deposit thickness with conservation of the microstructure was possible over a large range of electric fields and deposition times. No thickness limitation was observed in the investigated range of deposition times and electric fields without the need of any added ionic species. Besides, voltage measurements showed that the electric field over the suspension during the EPD process remains high, allowing continuous migration of Al particles to the coated electrode. Overall, the EPD process turned out to be an efficient way to adjust the deposit thicknesses up to 200 μm.

1. Introduction

Electrophoretic deposition studies started to appear during the XIX century. This process was first patented in 1933 by Harsanyi [1]. The patent concerned the electrophoretic deposition of tungsten and thorium oxide particles onto a platinum substrate.

Among all deposition techniques, the electrophoretic deposition (EPD) process displays numerous advantages, such as a low operating cost, relatively simple equipment and the ability to deposit uniformly onto complex parts [2]. EPD is an efficient process for the elaboration of homogeneous thickness and adjustable microstructure coatings on conductive substrates [3]. EPD can be used with a wide variety of particles: ceramic [4], metallic [5], graphite [6], graphene [7], carbon nanotube [8] and polymer particles [9].

In the literature, studies relative to metallic particle-based systems have been less reported than ceramic particle-based systems [10,11]. However, metallic materials can offer additional properties, such as magnetic, optical, electrical, catalytic, thermal, and mechanical properties [12–14]. Metallic particle deposits shaped by EPD reported in the literature include several metals such as gold [15,16], silver [17], platinum [5], nickel [18], titanium [19], iron [18], niobium [20] and aluminum [21]. Among these metal particles, aluminum (Al) particles exhibit peculiar properties: atmospheric corrosion resistance, high thermal and electrical conductivities, good mechanical properties for structural applications, and optical properties associated with a low density.

Many applications can take benefit of EPD deposition technique. The literature reports studies on the EPD of Al powder on magnesium alloys to enhance corrosion resistance [22,23] while maintaining a low density for lightweight structures [24–26]. Other studies have focused on the deposition of Al deposits to act as an intermediate catalyst carrier coating [27,28]. The fabrication of hydrophobic materials for water–oil separation by the EPD of Al nanoparticles on stainless steel mesh has also been reported [29]. The preparation of energetic materials — often referred to as nanothermites or metastable interstitial composites (MICs) — is also a field of investigation. MICs are prepared either by codeposition using EPD of Al nanoparticles with another type of nanoparticle, such as ZnO [30], CuO [31], Fe_2O_3 [32] or MoO_3 [33], or by coating nanostructures [34] with Al nanoparticles (composites). Investigations on MIC preparation represent the main contribution of the last 10 years

* Corresponding author.
E-mail address: pierre-louis.taberna@univ-tlse3.fr (P.-L. Taberna).

https://doi.org/10.1016/j.rinma.2022.100259
Received 3 September 2021; Received in revised form 13 January 2022; Accepted 25 January 2022
Available online 28 January 2022

of publications of all publications relative to the EPD of Al particles.

From a "process" point of view, studies generally reported the use of organic solvents for the preparation of Al powder suspensions (Fig. 1). This kind of solvent is advantageous for the EPD process because a significant voltage range can be investigated while avoiding water electrolysis and bubble formation at the electrodes. Moreover, metals such as Al present a high reactivity towards aqueous media. Thus, the choice of alcohols as dispersing media turns out to be more suitable. Indeed, even though the EPD of Al powder in alkaline aqueous media without organic resins has been reported [26], it leads to significant corrosion of the particles and important hydrogen development. These parasite reactions lead to the formation of defects in the deposits. Corrosion of the Al particles also induces a substantial increase in the ionic concentration in the suspension, which is known to be detrimental to the suspension stability and the EPD process. For these aforementioned reasons, organic solvents are preferred for such applications. Among organic solvents, alcohol-based solvents, such as ethanol and propan-2-ol, are widely reported in the literature, as shown in Fig. 1.

The EPD of Al powder is mostly carried out in ethanol media, as shown in Fig. 1 [25,27,35]. Nevertheless, the direct EPD of Al particles from a pure ethanol suspension is not possible [27], regardless of the applied voltage value [36]. Therefore, the addition of a cosolvent (acetylacetone [29], nitromethane) and/or ionic dispersants (polyelectrolytes, salts, acids) is necessary to obtain an Al particle deposits.

To compare with, the use of propan-2-ol-based suspensions is less referenced in the literature. Only a few studies mentioned the use of propan-2-ol as a base solvent for the EPD of Al powder [37]. The use of pure propan-2-ol, unlike pure ethanol, has been reported [36] to allow deposition to occur. However, the addition of a cosolvent, such as nitromethane [38], acetone [39], and acetylacetone [30], and/or polyelectrolytes, such as polethyleneimine [30,33], is sometimes found. However, to the best of our knowledge, no study evaluating the influence of the deposition time or the applied electric field on deposit properties (thickness, porosity, etc.) has been performed in pure propan-2-ol media. As no further addition of ionic dispersants is needed, the use of pure propan-2-ol could be interesting in obtaining thick deposits. Indeed, the thickness limitation in the EPD process is generally attributed to the presence of charging agents in the suspension leading to a high potential drop at the deposition electrode [40].

In this study, the feasibility of EPD from pure propan-2-ol suspensions without any other additives was evaluated. It has been shown that Al coatings were obtained from pure propan-2-ol suspensions, following a linear behavior with the increase of thickness as a function of the deposition time and the applied electric field. The deposits are porous, homogeneous and adherent with a voltage- and time-independent microstructure.

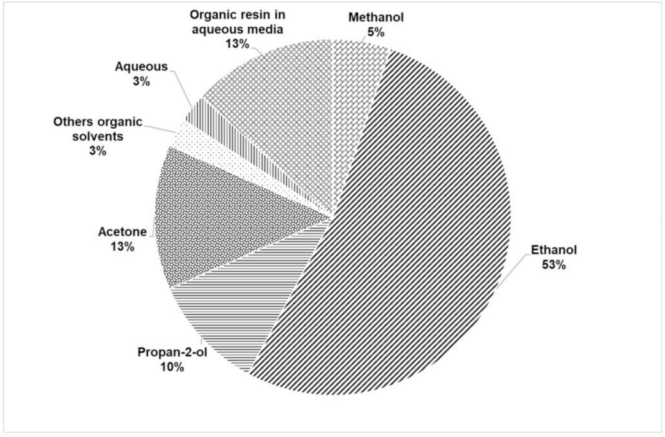

Fig. 1. Pie chart representing partitioning of base solvents used in the literature for EPD of Al powder.

2. Materials and methods

2.1. Materials

The substrate is a low-carbon 15CDV6 steel for which the composition is detailed in Table 1. Al powder (99.7%) with a spherical shape and an average size of 2 μm was provided by Toyal Europe Company. Propan-2-ol (ACS reagent ≥99.8%) was purchased from Sigma Aldrich (59,300 reference number) and used as received. To prepare the suspensions, Al powder was added to propan-2-ol, stirred for 30 min and sonicated for 20 min to disperse the particles. The Al particle concentration of the suspension was 10 g L^{-1}.

2.2. Powder analysis

To determine the size distribution of the Al powder, direct observation of the powder was performed with a MEB-FEG FEI Quanta 250 system. The oxide layer on the surface of particles was observed using a JEOL JEM 2100F-EDS TEM system. Specific surface measurements were performed with the one-point Brunauer, Emmett and Teller (BET) technique with nitrogen. Powder was degassed during 1 h at 90 °C then 2 h at 200 °C. The XRD pattern was acquired with an RX D4-Bruker-AXS diffractometer.

2.3. EPD process

EPD was performed in a two plane and parallel electrode cell (Fig. 2) with the substrate as the working cathode, a platinized titanium mesh as the anode and a 1050 aluminum wire as a quasi-reference. Distance between electrodes was kept constant to 30 mm. The coating area was a 30 mm diameter circle. The electrodes were adapted on a dip-coater setup to precisely control the withdrawal speed (10 mm min^{-1}) of the substrate from the suspension. The electrical supply was a Keithley 2611A SourceMeter system. Current response measurements were performed with an Agilent U1253B 4 ½ - Digit OLED handheld digital multimeter (1 measure per second).

Deposition time was varied from 0 to 20 min for a constant electric value of 10 Vcm^{-1}. Applied electric field was set from 0 to 60 Vcm^{-1} for a 10 min deposit duration.

2.4. Voltage measurement with a quasi-reference

The voltage measured between the deposition electrode and the 1050A quasi-reference electrode was recorded with a 1010E Gamry potentiostat interface, where the input impedance was greater than 10^{12} Ω. The quasi-reference electrode was placed 2 mm from the deposition electrode. The method is schematized in Fig. 3.

Assuming that neither electrode exhibits polarization resistance and that no voltage drop occurs at the counterelectrode, the cell applied voltage is described by the following expression as a function of the measured voltage:

$$U_{app} = U_{mes} + U_{susp} \quad (1)$$

where U_{app} is the applied voltage (V), U_{mes} is the measured voltage between the deposition electrode (V) and U_{susp} is the voltage drop over the corresponding suspension section.

2.5. Suspension characterizations

Conductivity measurements were performed with a Mettler Toledo Seven2Go Pro S7 conductivity meter with the conductivity probe "InLab 742-ISM", especially for low conductivity range measurements. Zeta potential and electrophoretic mobility measurements were performed with a Nanosizer ZS 90 Malvern setup.

Table 1
Chemical composition of 15CDV6 steel (range in weight %).

C	P	Si	V	Mn	S	Cr	Mo	Fe
0.12–0.18	0.02 max	0.20 max	0.20–0.30	0.08–1.10	0.015 max	0.25–1.5	0.80–1.00	Bal

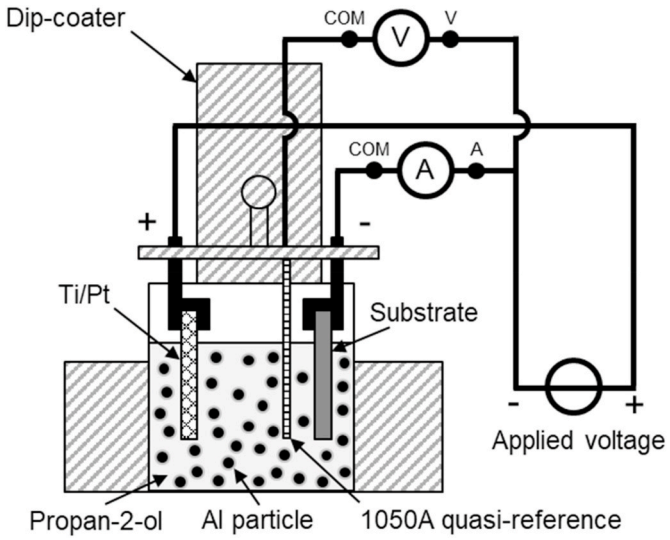

Fig. 2. Schematic representation of the experimental deposition setup.

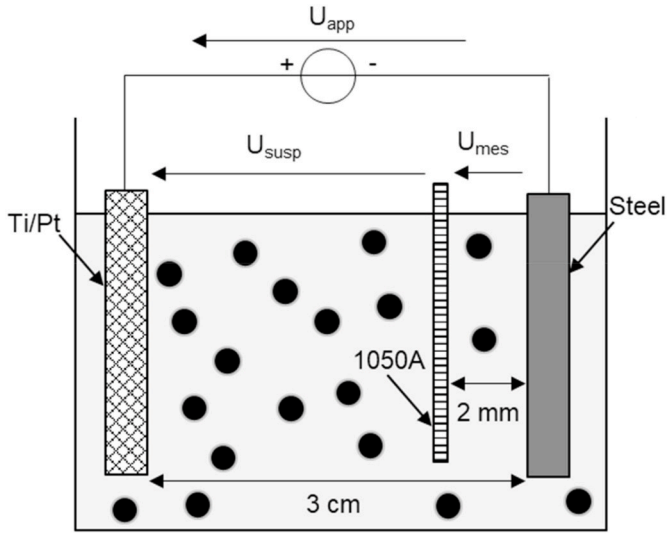

Fig. 3. Schematic representation of the voltage measurement between the deposition electrode (steel) and the quasi-reference electrode (1050A).

2.6. Deposit microstructure characterization

Microstructural observations were performed with scanning electron microscopy with a field emission gun (SEM-FEG): MEB/FIB Helios 600i – EDS. Thicknesses of the deposit were measured from SEM cross-section observations.

Epoxy resin impregnation was performed under pressure in the deposits to make a contrast agent for porosity determination. Samples were polished by using the Ar^{+} ion beam of a cross-section polisher device (JEOL IB-19510 CP). Porosity measurements were performed by SEM image analysis with ImageJ software.

3. Results and discussion

3.1. Al particle analysis

The XRD pattern of the commercial powder used for this study is presented in Fig. 4 (A). All the peaks are indexed as the Al phase (JCPDS 04–0787 card).

As observed in Fig. 4 (B), the Al powder exhibits a volume distribution corresponding to a mean diameter of approximately 2 µm. A d_V50 of 1.8 µm is calculated. The specific surface area measured from gas sorption analysis using the BET model is 1.9 ± 0.1 m^2 g^{-1}. This value is in good agreement with the value of 1.8 m^2 g^{-1} obtained for a 5 µm Al powder according to Yang et al. [27]. The surface of Al is naturally covered by a native oxide layer [41]. The thickness of the native oxide layer on the particle surface was measured by TEM observation (Fig. 5).

As presented in Fig. 5, the Al particles are composed of two different parts, a core and a surface oxide layer. The Al core is homogenous and displays atomic planes, proving its crystalline structure. The surface layer, attributed to natural aluminum oxide, is 3 nm thick. This measurement is consistent with the 2–5 nm thickness range reported by Bocanegra [42] for different Al powder types. From the TEM image, the oxide layer could be amorphous, as it is generally reported in the literature that Al is naturally covered by an amorphous oxide layer at low temperature [43,44].

3.2. EPD conditions and characteristics

The zeta potential of Al particles in a propan-2-ol suspension estimated from a zetameter instrument is 34 ± 20 mV. The standard deviation is relatively high, which is inherent to the propan-2-ol medium. Indeed, propan-2-ol suspensions exhibit low relative dielectric permittivity involving very low surface charges. The zeta potential of Al in propan-2-ol suspensions is inconsistent in the literature. The only result comes from Zhu et al. [33]: a zeta potential value of approximately 5 mV was measured for 50 nm Al particles dispersed in pure propan-2-ol [33]. As the chemical surface similarities of the two different Al powders cannot be confirmed, it is difficult to determine the difference in values. Moreover, the limited accuracy of zeta potential determination in propan-2-ol-based suspensions is arguable because of their poor conductivity (<0.1 µScm^{-1} in a 10 g L^{-1} Al suspension). Therefore, only the signs of the zeta potentials are similar. Herein, a positive value indicates that EPD should occur at the cathode electrode.

The electric field and time are the two main parameters controlling the EPD process. At a 10 min duration, Al coatings exhibit good uniformity and cover a wide range of electric fields, from 5 to 60 Vcm^{-1}. On the other hand, at 10 Vcm^{-1}, the deposits are homogenous for a wide range of deposition times, from 3 to 20 min.

As presented in Fig. 6 (A), the surface deposit morphology is even and composed of a wide range of Al particle sizes, corresponding to the powder size distribution. Therefore, deposition of particles of fairly different sizes can be achieved concomitantly by using a propan-2-ol suspension. Cross-sections of deposits prepared by FIB ablation (Fig. 6 (B)) show a homogeneous and relatively porous coating. The cross-sectional observation shows that the deposit levels differ from the initial topography of the substrate, even if the contact between Al particles and steel is observed.

The aim of this work is to study the influence of EPD process parameters, such as deposition time and applied electric field, on the deposition kinetics and coating morphology.

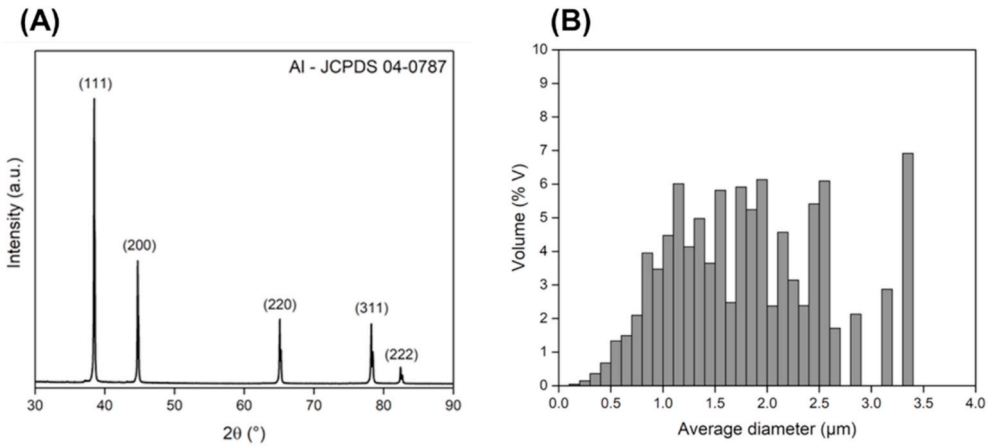

Fig. 4. (A) XRD pattern of commercial Al powder, (B) volume distribution of Al particles. Analysis performed on 981 particles.

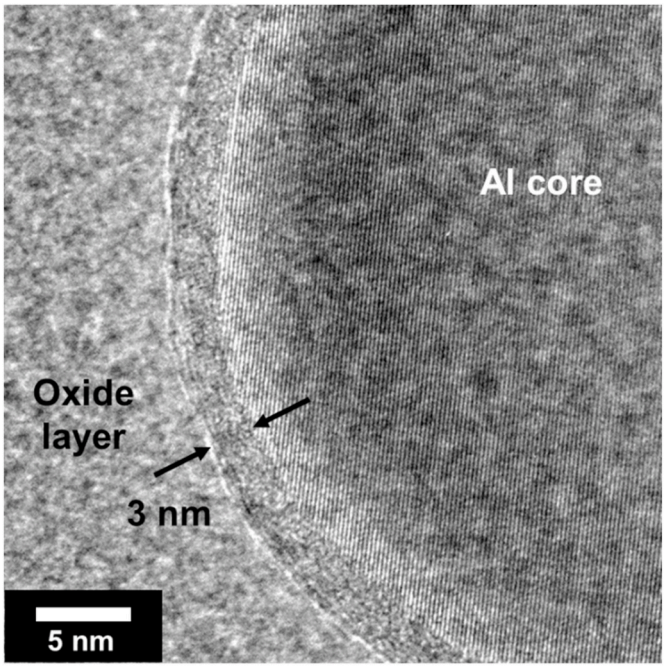

Fig. 5. TEM image of a 57 nm Al particle.

3.3. *Influence of the deposition time on the deposition rate and coating morphology*

The deposition time was set from 3 to 20 min. The evolution of the deposit thickness versus time is reported in Fig. 7 for a constant electric field value of 10 Vcm^{-1}. From 3 to 20 min, the thickness increases and follows a linear-like shape from 10 to 80 μm. The slope extracted from the linear fit is 4.4 μm min^{-1}.

No thickness limitation was observed within the time range studied. Consequently, the critical time, corresponding to the moment when the deposition rate starts to decrease, appears to be higher than the longer deposition time tested (*i.e.,* 20 min). The deposition rate decrease is generally attributed to either the depletion of particles in the suspension close to the deposited electrode [45] or to an increase in the electrical

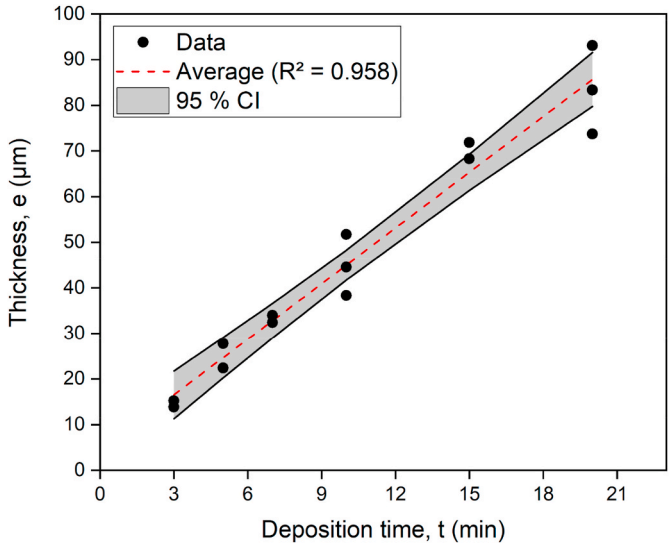

Fig. 7. Evolution of deposit thickness as a function of the deposition time for an applied electric field fixed at 10 Vcm^{-1}. "95% CI" represents the 95% Confidence Interval extracted from the linear fit.

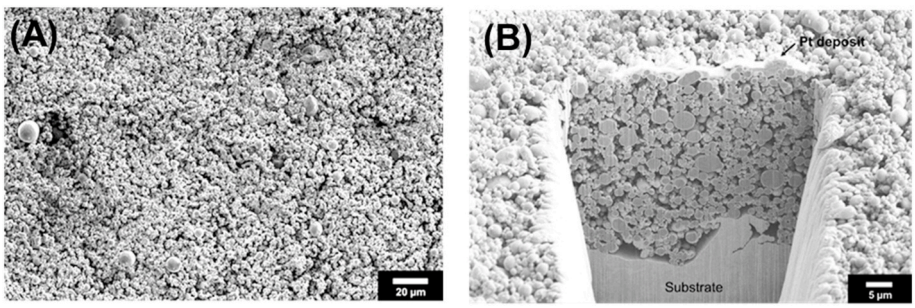

Fig. 6. (A) Surface and (B) cross-section of the Al coating deposited at 10 Vcm^{-1} in 10 min from the propan-2-ol suspension.

resistivity of the deposit [46]. This latter point is associated with a decrease in the electric field in the suspension limiting particle migration.

The critical time for deposition can be defined as the duration for which the deposition rate starts to decrease. Table 2 gives an overview of the critical time determined for the deposition of Al particles in ethanol-based suspensions with the addition of aluminum chloride salt. In this configuration, the critical time is generally shorter than 2 min for Al particles.

As previously indicated, the EPD of Al particles is not possible from a pure ethanol suspension, and the addition of a metallic salt such as aluminum chloride is often reported [24,28,35]. The dissolution of ionic species involves an increase in the suspension conductivity and the deposition rate. Regarding deposition performed in pure propan-2-ol, the deposition rate was lower than that in ethanol suspensions. However, the areal deposit mass reached (11 $mgcm^{-2}$) is significantly higher and could hypothetically be even higher for deposition times longer than 20 min. The low areal deposit mass of the $AlCl_3$ ethanol suspension could be attributed to the higher potential drop at the deposition electrode, which rapidly limits the EPD process. A larger potential drop at the deposition electrode implies a very low electric field across the suspension, which prevents particle migration to the substrate.

To understand the absence of thickness limitations, the measurement of the voltage between the deposition electrode and a quasi-reference electrode was performed.

Fig. 8 presents the voltage drop over the 2.8 cm suspension section U_{susp} divided by the applied voltage as a function of the deposition time. The voltage drop over the suspension starts to decrease from approximately 96% of the applied voltage for short deposition times. The voltage ratio decreases slowly with time to reach a value of 85% after 10 min. The potential drop over the suspension tends to remain relatively constant for a longer time. This result proves that the applied voltage is almost entirely located in the suspension part. Consequently, the Al particles can continuously migrate from the suspension toward the deposition electrode. The deposit can grow continually as long as there is no significant particle depletion in the suspension. This explains why no decrease in the deposition rate is observed over time, as shown in Fig. 7.

The high electric field over the suspension also means that no or a low potential drop at the substrate electrode is present. Indeed, the existence of a potential drop at the deposition electrode has been mentioned in the literature [47] for different systems. The potential drop is generally related to the nature of the suspension medium and notably to the presence of dissolved ionic species [48]. For instance, Anné et al. [48] reported a larger potential drop with the presence of charging additives in an ethanol-based suspension of Al_2O_3 compared to a methyethylketone – butylamine suspension without the addition of ionic dispersants. Therefore, for the $AlCl_3{\cdot}6H_2O$ ethanol-based suspensions reported in the literature (Table 2), the presence of dissolved ions in the suspension leads to the existence of a potential drop at the deposition electrode [47]. In this case, the ratio between suspension resistance and deposit resistance tends to be low [40]. Several models have tried to explain the origin of the potential drop at the deposition electrode by considering the presence of ionic species in the suspension: the Van Tassel ion depletion model [49] and interparticle interactions in the deposit model [50] are generally found. Regardless of the precise origin of the deposit potential drop, in the case of a suspension containing ionic species, the electric field over the suspension rapidly decreases, limiting the migration of Al particles. This explains the rapid mass limitations (*i.e.,* short critical time <2 min) observed in the $AlCl_3{\cdot}6H_2O$ ethanol-based systems reported in the literature (Table 2). In contrast, the absence of added ions in the propan-2-ol suspension does not create a potential drop at the deposition electrode and allows us to keep a very high electric field strength in the suspension. By ensuring continuous migration of Al particles to the deposition electrode, the use of a pure propan-2-ol suspension appears to be interesting to obtain a high-thickness deposit.

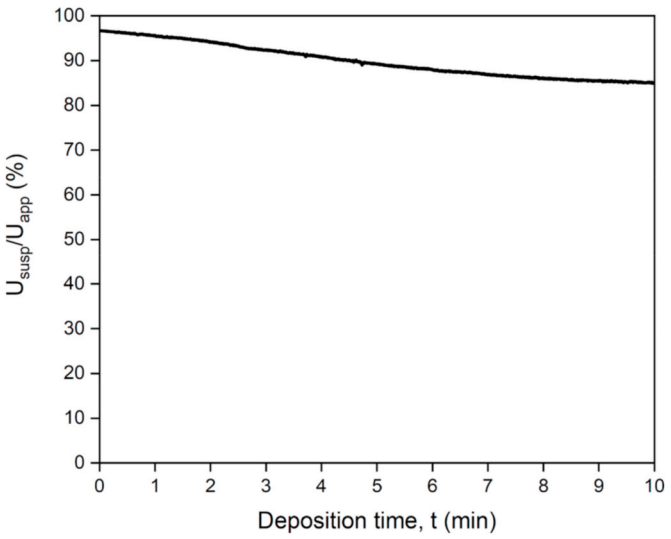

Fig. 8. Voltage drop across the suspension divided by the applied voltage (%) as a function of the deposition time. Applied voltage is 30 V (E = 10 Vcm^{-1}).

Fig. 9 (A) and (B) present cross-section SEM images of coatings obtained for EPD carried out for 5 and 15 min, respectively, in propan-2-ol at 10 Vcm^{-1}. The increase in deposition time leads to an increase in the deposit thickness. The morphologies of these two deposits are also interesting and appear to be similar, with a wide range of particle sizes within the coatings, corresponding to the powder size distribution. This tendency is confirmed by the porosity measurements presented in Fig. 10. The curve shows that the porosities of the coatings are similar, with a range of 50–60% for all deposition times at 10 Vcm^{-1}. No specific gradient of porosity was observed in the deposit thickness, demonstrating that the microstructure of the coating was homogenous from the substrate/deposit interface up to the outer surface of the coating.

Based on the results previously presented, some major conclusions can be drawn. The EPD of Al powder from the pure propan-2-ol suspension appears to be a technique that can finely control the deposit thickness, with maximum thicknesses ranging up to 100 μm. The microstructure organization and porosity rate seem to be independent of the deposition time. The use of the propan-2-ol suspension can lead to a higher areal deposit mass than the use of ethanol-based suspensions. The high thickness reachable is associated with the absence of a potential drop at the deposition electrode.

Table 2
Critical time in ethanol-based suspensions reported in the literature.

	This study	Kuwano [35]	Yang [28]		
Medium	Propan-2-ol	Ethanol	Ethanol		
Metallic salt nature	–	$AlCl_3$	$AlCl_3{\cdot}6H_2O$		
Metallic salt concentration (mM)	–	2.5	0.5		
Al particle shape	Spherical				
Al particle size (μm)	2	–	2		
Al particle concentration (gL^{-1})	10				
Applied electric field (Vcm^{-1})	10	43	20	30	40
t critical (min)	>20	1	2	1.7	1.3
Thickness (μm)	>80	–	20.2	32.2	51.6
Deposition rate ($\mu m min^{-1}$)	4	–	10	19	40
Porosity (%)	53	–	37.8	49.4	56.9
Areal deposit mass ($mgcm^{-2}$)	>11	7	3.4	4.4	6
Mass rate per electric field ($\mu gcm^{-1}V^{-1}s^{-1}$)	0.9	2.7	1.4	1.5	1.9

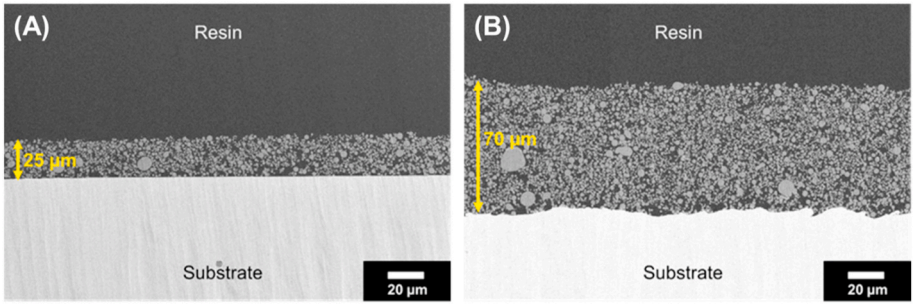

Fig. 9. Cross-section of the Al coating deposited for (A) 5 min and (B) 15 min at 10 Vcm^{-1} from the pure propan-2-ol suspension, prepared with a cross-section polisher machine.

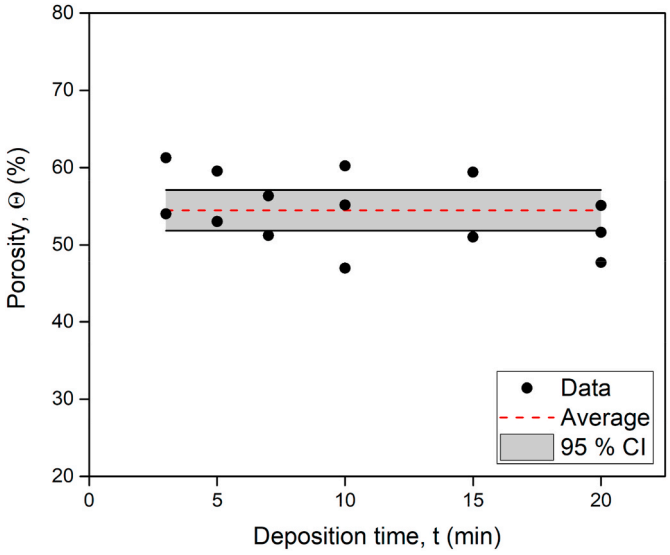

Fig. 10. Evolution of the coating porosity as a function of the deposition time at 10 Vcm^{-1} in pure propan-2-ol. "95% CI" represents the 95% Confidence Interval extracted from the average.

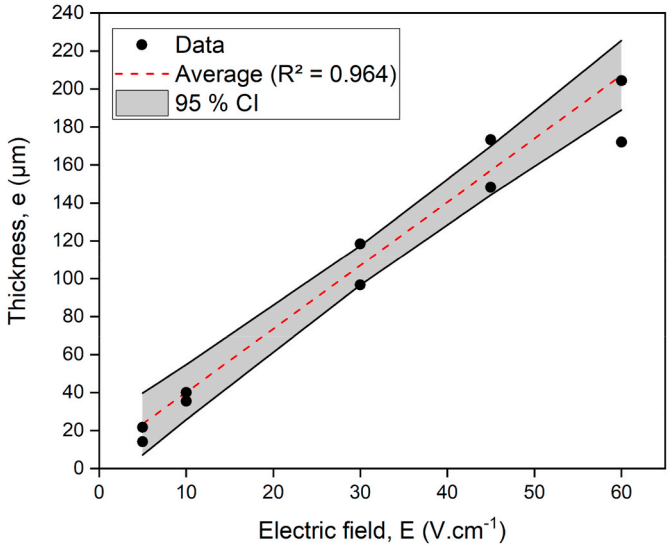

Fig. 11. Evolution of coating thickness as a function of applied electric field for a deposition time of 10 min "95% CI" represents the 95% Confidence Interval extracted from the linear fit.

3.4. *Influence of the applied electric field on the deposition kinetics and coating morphology*

The electric field influence has been studied in a range from 5 to 60 Vcm^{-1} and for a 10 min deposit duration. The evolution of the deposit thickness as a function of the applied electric field is shown in Fig. 11. The thickness of the deposit linearly increases with the applied electric field in a range up to 60 Vcm^{-1}. The corresponding thickness varies from 20 to 200 µm. This behavior is generally mentioned in the literature as it follows the Hamaker relationship [51].

As shown in Fig. 12, the porosity of deposits remains constant for all applied electric field values in the range of 5–60 Vcm^{-1}. This highlights that the porosity of deposits is independent of the electric field value for the pure propan-2-ol system. The porosity values presented in Fig. 12 are on the same order of magnitude as the porosity range displayed in Fig. 10. This demonstrates that the deposit porosity does not significantly depend on the deposition time and the applied electric field.

Fig. 13 (A) and (B) present the SEM cross-section images of the coatings deposited at 10 and 30 Vcm^{-1} for 10 min, respectively. From these microstructural observations, the porosities are similar for those two electric fields. Moreover, the porosity distribution appears to be homogenous in the deposit thickness, and no agglomeration phenomenon is visible. These results are different from those reported in Table 2, which show that porosity is greatly influenced by the electric field for $AlCl_3{\cdot}6H_2O$ ethanol-based systems. Indeed, the higher the applied electric field is, the more porous the coatings according to L. Yang et al.

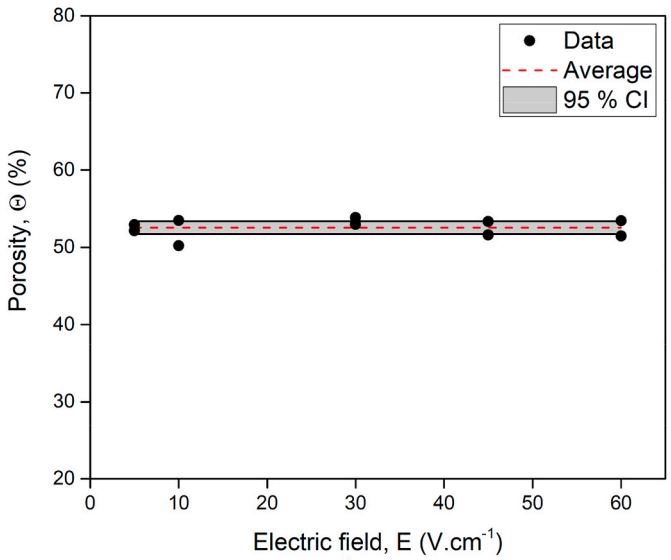

Fig. 12. Evolution of coating porosity as a function of applied electric field. "95% CI" represents the 95% Confidence Interval extracted from the average.

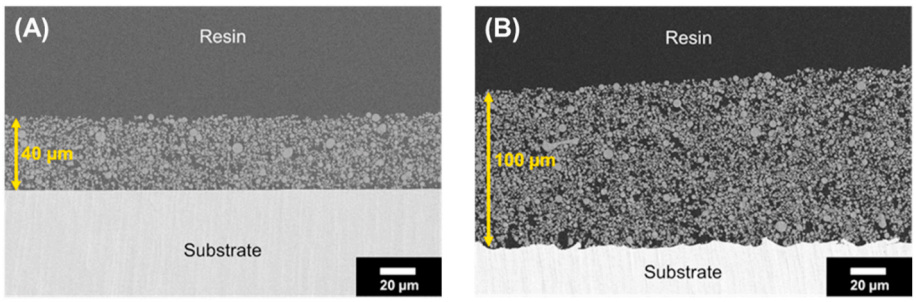

Fig. 13. Cross-section of the Al coating deposited at (A) 10 Vcm^{-1} and (B) 30 Vcm^{-1} for 10 min from the pure propan-2-ol suspension, prepared with a cross-section polisher machine. Image used for porosity measurement.

[28].

Different authors attributed the increase in porosity rate to the too rapid migration of particles under a high voltage field, which leads to inhomogeneous deposits [28,52,53]. Even if the electrophoretic mobility of Al particles in pure propan-2-ol is lower (0.9 $\mu mcmV^{-1}s^{-1}$) than that of $AlCl_3{\cdot}6H_2O$ ethanol particles (1.5 $\mu mcmV^{-1}s^{-1}$) [28], this cannot explain why the porosity obtained from the pure propan-2-ol suspension is constant from 5 to 60 Vcm^{-1} while the porosity increases with electric fields for the $AlCl_3{\cdot}6H_2O$ ethanol systems. An increase in the electric field value leads to a growing electrochemical reaction rate [49]. These parasite reactions could induce a uniform decrease in the deposit and lead to local suspension destabilization caused by pH variation involving agglomeration phenomena. The presence of ionic species from $AlCl_3{\cdot}6H_2O$ could strongly affect the deposition process at high electric field values. Furthermore, as the conductivity of the $AlCl_3{\cdot}6H_2O$ ethanol-based suspension is higher than that of pure propan-2-ol, higher local heating from the Joule effect in the ethanol-based suspension could also explain the increase in deposit heterogeneity with an electric field.

The absence of added ions in propan-2-ol is interesting for several reasons. First, it prevents the formation of a potential drop at the deposition electrode. The voltage across the suspension is close to the applied voltage. Consequently, the Al particles can continuously migrate from the suspension to the deposition electrode, and it is possible to obtain a very thick deposit. The unique limitation seems to be the particle concentration in the suspension. Second, the absence of charging agents allows the microstructure to be independent of the applied electric field. Therefore, the use of a pure propan-2-ol suspension is interesting in reducing the preparation time. Indeed, for a constant deposition time, the applied electric field increases with the deposit thickness, and the same porosity range is maintained.

3.5. Evaluation of the EPD process

An effective way to combine deposition results obtained in this study, either by varying the deposition time or the electric field, is to calculate the charge passed during deposition. The surface passed charge can be easily calculated by integrating the current density as a function of the time curves. Consequently, deposit thickness has been plotted as a function of the passed charge for all deposition experiments presented in this work (Fig. 14).

Regardless of the deposition time and the electric field values used, Fig. 14 clearly shows that the deposit thickness increases linearly with the passed charge, as predicted in the Hamaker model [51]. The linearity of this curve plotted using all the deposition experiments presented in this work ensures that the EPD of Al particles from pure propan-2-ol suspensions is a robust and reliable technique. It also shows that as the microstructure is independent of the process parameters, the desired deposit thickness is reachable either by adjusting the deposition time or the applied electric field. This specificity allows for the EPD of Al particles from a pure propan-2-ol suspension, an adaptable and versatile process.

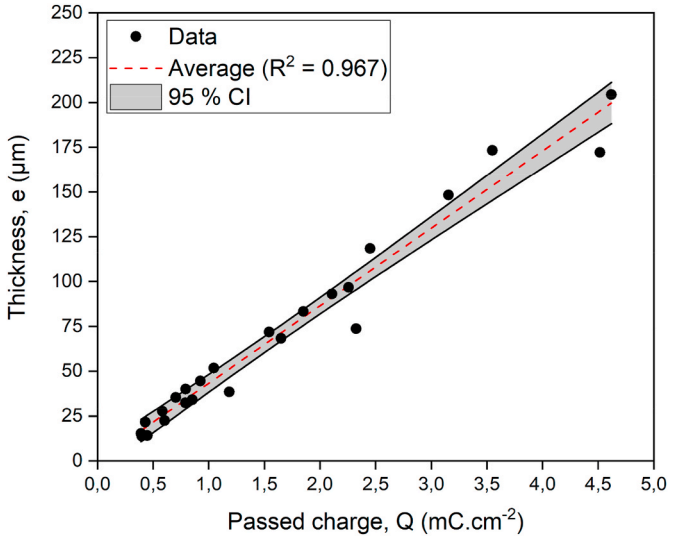

Fig. 14. Evolution of the deposit thickness as a function of the passed charge for all deposition experiments performed in this study. "95% CI" represents the 95% Confidence Interval extracted from the linear fit.

4. Conclusions and perspectives

The EPD of Al particles from pure propan-2-ol suspensions onto steel plates has been performed, which is quite innovative. Uniform deposits with good coverage are obtained over a wide range of deposition times and applied electric fields. A key point is that no thickness limitation is observed in the investigated range of EPD parameters. Voltage measurements performed with a quasi-reference during the EPD process show that the voltage drop over the suspension remains high (over 85% of the applied voltage), even for long deposition times, allowing continuous migration from the suspension to the deposition electrode. Consequently, for this propan-2-ol suspension composition, without the addition of ionic species, the deposition electrode presents very little potential drop, leading to a very thick deposit. These results differ from those of $AlCl_3{\cdot}6H_2O$ ethanol-based systems previously reported in the literature, which present rapid thickness limitations due to a higher potential drop at the deposition electrode because of the presence of ionic species. Even if the deposition rate is lower than that of those systems, the areal deposited mass obtained from pure propan-2-ol is higher, and a thickness up to 200 µm could be achieved from a long deposition time and a high applied electric field. The porosity rate of all the deposits obtained with a wide range of deposition times and applied fields remains constant from 50 to 60%. This demonstrates that the EPD of Al powder from pure propan-2-ol allows precise control of the coating

thickness without a significant microstructure change. This means that the desired thickness can be reached either by varying the deposition time or the electric field. This feature makes this EPD process adaptable and versatile.

Data availability

Due to the sensitive nature of this work, the data will remain confidential and will not be shared.

Credit author statement

Julien Wagner: Conceptualization, Methodology, Validation, Investigation, Writing - Original Draf. Claudie Josse: Resources, Validation, Methodology. Léa Gani: Funding acquisition, Writing – review & editing. Stéphane Knittel: Funding acquisition, Writing – review & editing. Pierre-Louis Taberna: Resources, Writing – original draft, Supervision, Project administration. Florence Ansart: Resources, Writing – original draft, Supervision, Project administration.

Declaration of competing interest

The authors declare that they have no known competing financial interests or personal relationships that could have appeared to influence the work reported in this paper.

Acknowledgments

The authors would like to thank Safran Aircraft Engines (Site Evry-Corbeil, France) and the ANRT (no2018/0917, France) for financial support. The authors are also grateful to the UAR 3623 Centre de Microcaractérisation Raimond Castaing (Toulouse, France) for SEM and TEM observations.

References

[1] E. Harsanyi, Method of Coating Radiant Bodies, 1933. US1897902.
[2] G. Pujol, Elaboration par voie sol-gel de nouvelles barrières thermiques architecturées présentant des propriétés contre l'infiltration des oxydes CMAS (Ca, Mg, Al, Si) - Etude de la réparabilité de systèmes endommagés, Université de Toulouse 3 Paul Sabatier, 2014.
[3] L. Besra, M. Liu, A review on fundamentals and applications of electrophoretic deposition (EPD), Prog. Mater. Sci. 52 (1) (2007) 1–61, https://doi.org/10.1016/j.pmatsci.2006.07.001.
[4] I. Corni, M.P. Ryan, A.R. Boccaccini, Electrophoretic deposition: from traditional ceramics to nanotechnology, J. Eur. Ceram. Soc. 28 (7) (2008) 1353–1367, https://doi.org/10.1016/j.jeurceramsoc.2007.12.011.
[5] T. Teranishi, M. Hosoe, T. Tanaka, M. Miyake, Size control of monodispersed Pt nanoparticles and their 2D organization by electrophoretic deposition, J. Phys. Chem. B 103 (19) (2002) 3818–3827, https://doi.org/10.1021/jp983478m.
[6] K. Ui, N. Koura, Fabrication and application of carbon material films by electrophoretic deposition method, J. Jpn. Soc. Powder Powder Metall. 55 (1) (2008) 35–43.
[7] Y. Ma, J. Han, M. Wang, X. Chen, S. Jia, Electrophoretic deposition of graphene-based materials: a review of materials and their applications, J. Mater. 4 (2) (2018) 108–120, https://doi.org/10.1016/j.jmat.2018.02.004.
[8] A.R. Boccaccini, et al., The electrophoretic deposition of inorganic nanoscaled materials, J. Ceram. Soc. Japan 114 (1325) (2006) 1–14, https://doi.org/10.2109/jcersj.114.1.
[9] B. Fori, P.L. Taberna, L. Arurault, J.P. Bonino, Decisive influence of colloidal suspension conductivity during electrophoretic impregnation of porous anodic film supported on 1050 aluminium substrate, J. Colloid Interface Sci. 413 (2014) 31–36, https://doi.org/10.1016/j.jcis.2013.08.011.
[10] I. Zhitomirsky, A. Petric, Electrophoretic deposition of ceramic materials for fuel cell applications, J. Eur. Ceram. Soc. 20 (12) (2000) 2055–2061, https://doi.org/10.1016/S0955-2219(00)00098-4.
[11] B. Ferrari, A.J. Sanchez-Henrencia, R. Moreno, Electrophoretic forming of Al2O3/Y-TZP layered ceramics from aqueous suspensions, Mater. Res. Bull. 33 (3) (1998) 487–499, https://doi.org/10.1016/S0025-5408(97)00244-4.
[12] I.D. Morokhov, V.I. Petinov, L.I. Trusov, V.F. Petrunin, Structure and properties of fine metallic particles, Sov. Phys. Usp. 24 (4) (1981) 295–317, https://doi.org/10.1070/PU1981v024n04ABEH004800.
[13] Y. Volokitin, J. Sinzig, L.J. de Jongh, G. Schmid, M.N. Vargaftik, I.I. Moiseev, Quantum-size effects in the thermodynamic properties of metallic nanoparticles, Nature 384 (1996) 621–623, https://doi.org/10.1038/384621a0.
[14] J.T. Lue, A review of characterization and physical property studies of metallic nanoparticles, J. Phys. Chem. Solid. 62 (9–10) (2001) 1599–1612, https://doi.org/10.1016/S0022-3697(01)00099-3.
[15] S.Q. Zhu, T. Zhang, X.L. Guo, Q.L. Wang, X. Liu, X.Y. Zhang, Gold nanoparticle thin films fabricated by electrophoretic deposition method for highly sensitive SERS application, Nanoscale Res. Lett. 7 (2012) 1–7, https://doi.org/10.1186/1556-276X-7-613.
[16] S.L. Allen, F.P. Zamborini, Size-selective electrophoretic deposition of gold nanoparticles mediated by hydroquinone oxidation, Langmuir 35 (2019) 2137–2145, https://doi.org/10.1021/acs.langmuir.8b03904.
[17] M. Zarbov, D. Brandon, L. Gal-Or, N. Cohen, EPD of metallic silver particles: problems and solutions, Key Eng. Mater. 314 (2009) 95–100, https://doi.org/10.4028/www.scientific.net/kem.314.95.
[18] K. Luo, N. Shi, H. Cong, C. Sun, Electrophoretic deposition of nickel, iron and aluminum nanoparticles on carbon fibers, J. Solid State Electrochem. 10 (12) (2006) 1003–1007, https://doi.org/10.1007/s10008-005-0044-4.
[19] K.T. Lau, C. Sorrell, Effect of charging agents on electrophoretic deposition of titanium particles, J. Aus. Ceram. Soc. 49 (2) (2013) 104–112.
[20] C.P. Gutierrez, J.R. Mosley, T.C. Wallace, Electrophoretic deposition: a versatile coating method, J. Electrochem. Soc. 109 (10) (1962) 923, https://doi.org/10.1149/1.2425207.
[21] F. Pearlstein, R. Wick, A. Gallaccio, Electrophoretic deposition of metals, J. Electrochem. Soc. (1963) 843–846.
[22] A. Shahriari, H. Aghajani, S. Fazlinejad, A study of corrosion behavior of 3YSZ coating on AZ91D alloy different interlayers, Eur. Corros. Congr. EUROCORR 4 (2016) 2522–2535, 2016.
[23] A. Shahriari, H. Aghajani, Electrophoretic deposition of 3YSZ coating on AZ91D alloy using Al and Ni-P interlayers, J. Mater. Eng. Perform. 25 (10) (2016) 4369–4382, https://doi.org/10.1007/s11665-016-2253-7.
[24] H. Aghajani, M. Pouzesh, Electrophoretic deposition and corrosion behavior study of aluminum coating on AZ91D substrate, J. Part. Sci. Technol. 3 (2017) 219–232, https://doi.org/10.22104/JPST.2018.2662.1105.
[25] A. Shahriari, H. Aghajani, Electrophoretic deposition of 3YSZ coating on AZ91D using an aluminum interlayer, Protect. Met. Phys. Chem. Surface 53 (3) (2017) 518–526, https://doi.org/10.1134/S2070205117030212.
[26] G. Knörnschild, Electrophoretic deposition of aluminum on an Mg-alloy, Rev. Matéria 10 (3) (2005) 497–501.
[27] K.S. Yang, Z. Jiang, J.S. Chung, Electrophoretically Al-coated wire mesh and its application for catalytic oxidation of 1,2-dichlorobenzene, Surf. Coating. Technol. 168 (2–3) (2003) 103–110, https://doi.org/10.1016/S0257-8972(02)00569-8.
[28] L. Yang, X. Wu, D. Weng, Development of uniform and porous Al coatings on FeCrAl substrate by electrophoretic deposition, Colloids Surfaces A Physicochem. Eng. Asp. 287 (1–3) (2006) 16–23, https://doi.org/10.1016/j.colsurfa.2006.03.016.
[29] Z. Xu, D. Jiang, Z. Wei, J. Chen, J. Jing, Fabrication of superhydrophobic nano-aluminum films on stainless steel meshes by electrophoretic deposition for oil-water separation, Appl. Surf. Sci. 427 (2018) 253–261, https://doi.org/10.1016/j.apsusc.2017.08.189.
[30] X. Guo, T. Liang, J. Wang, X. Li, Facilely electrophoretic derived aluminum/zinc (II) oxide nanocomposite with superhydrophobicity and thermostability, Ceram. Int. (2019), https://doi.org/10.1016/j.ceramint.2019.09.071, 0–1.
[31] K.T. Sullivan, M.A. Worsley, J.D. Kuntz, A.E. Gash, Electrophoretic deposition of binary energetic composites, Combust. Flame 159 (6) (2012) 2210–2218, https://doi.org/10.1016/j.combustflame.2012.01.021.
[32] D. Zhang, X. Li, B. Qin, C. Lai, X. Guo, Electrophoretic deposition and characterization of nano-Al/Fe 2O3 thermites, Mater. Lett. 120 (2014) 224–227, https://doi.org/10.1016/j.matlet.2014.01.113.
[33] Y. Zhu, et al., Tuning the surface charges of MoO3 by adsorption of polyethylenimine to realize the electrophoretic deposition of high-exothermic Al/MoO3 nanoenergetic films, Mater. Des. 109 (2016) 652–658, https://doi.org/10.1016/j.matdes.2016.07.109.
[34] X. Zhou, X. Ke, W. Jiang, Aluminum/copper oxide nanostructured energetic materials prepared by solution chemistry and electrophoretic deposition, RSC Adv. 6 (96) (2016) 93863–93866, https://doi.org/10.1039/c6ra20739a.
[35] S. Kuwano, T. Yamada, Mechanism of electrophoretic deposition of aluminum powder from suspension in ethylalcohol, J. Met. Finish Soc. Jpn. 29 (11) (1978) 584–589.
[36] D.R. Brown, F.W. Salt, The mechanism of electrophoretic deposition, J. Appl. Chem. 15 (1965) 40–48, https://doi.org/10.1002/jctb.5010150505.
[37] E.S. Leonenko, L.I. Sorokina, R.M. Ryazanov, E.A. Lebedev, Features of electrophoretic formation of local heat sources based on nanosized powder Al, J. Phys. Conf. Ser. 2086 (1) (2021), https://doi.org/10.1088/1742-6596/2086/1/012192, 012192.
[38] R.J. Pearce, R.D. Giles, L.E. Tavender, Preparation and properties of UAlx coatings formed on uranium via the electrophoretic deposition of aluminium powder, J. Nucl. Mater. 24 (1967) 129–140.
[39] N. Askari, M. Yousefpour, M. Rajabi, Electrochemical and biological characterization HA/Al2O3-YSZ nano-composite coatings using electrophoretic process, J. Biomed. Mater. Res. 106 (7) (2018) 1916–1922, https://doi.org/10.1002/jbm.a.36392.
[40] G. Anné, B. Neirinck, K. Vanmeensel, O. Van Der Biest, J. Vleugels, Origin of the potential drop over the deposit during electrophoretic deposition, J. Am. Ceram. Soc. 89 (3) (2006) 823–828, https://doi.org/10.1111/j.1551-2916.2005.00817.x.
[41] M. Pourbaix, Atlas D'équilibres Électrochimiques, Gauthiers-Villars & Cie, 1963.

[42] P. Bocanegra, Études expérimentales et modélisation de la combustion des nuages de particules micrométriques et nanométriques d'aluminium, Université d'Orléans, 2007.
[43] A.F. Beck, M.A. Heine, E.J. Caule, M.J. Pryor, The kinetics of the oxidation of Al in oxygen at high temperature, Corrosion Sci. 7 (1) (1967), https://doi.org/10.1016/s0010-938x(67)80066-0.
[44] H.J. van Beek, E.J. Mittemeijer, Amorphous and crystalline oxides on aluminium, Thin Solid Films 122 (2) (1984) 131–151, https://doi.org/10.1016/0040-6090(84)90004-X.
[45] P. Sarkar, P.S. Nicholson, Electrophoretic deposition (EPD): mechanisms, kinetics, and application to ceramics, J. Am. Ceram. Soc. 79 (8) (1996) 1987–2002, https://doi.org/10.1111/j.1151-2916.1996.tb08929.x.
[46] B. Ferrari, R. Moreno, J.A. Cuesta, A resistivity model for electrophoretic deposition, Key Eng. Mater. 314 (2006) 175–180, https://doi.org/10.4028/www.scientific.net/KEM.314.175.
[47] L. Stappers, L. Zhang, O. Van Der Biest, J. Fransaer, Study of the deposit resistance during electrophoretic deposition, Key Eng. Mater. 412 (2009) 9–14, https://doi.org/10.4028/www.scientific.net/KEM.412.9.
[48] G. Anné, K. Vanmeensel, J. Vleugels, O. Van Der Biest, Influence of the suspension composition on the electric field and deposition rate during electrophoretic deposition, Colloids Surfaces A Physicochem. Eng. Asp. 245 (1–3) (2004) 35–39, https://doi.org/10.1016/j.colsurfa.2004.07.001.
[49] J.J. Van Tassel, C.A. Randall, Role of ion depletion in the electrophoretic deposition of alumina powder from ethanol with increasing quantities of HCl, J. Mater. Sci. 41 (24) (2006) 8031–8046, https://doi.org/10.1007/s10853-006-0770-8.
[50] G. Anné, B. Neirinck, K. Vanmeensel, O. Van der Biest, J. Vleugels, Influence of electrostatic interactions in the deposit on the electrical field strength during electrophoretic deposition, Key Eng. Mater. 314 (2006) 181–186, https://doi.org/10.4028/www.scientific.net/kem.314.181.
[51] H.C. Hamaker, Formation of a deposit by electrophoresis, Trans. Faraday Soc. 35 (1940) 279–287, https://doi.org/10.1039/TF9403500279.
[52] S.J. Limmer, T.P. Chou, G.Z. Cao, A study on the influences of processing parameters on the growth of oxide nanorod arrays by sol electrophoretic deposition, J. Sol. Gel Sci. Technol. 36 (2) (2005) 183–195, https://doi.org/10.1007/s10971-005-3548-6.
[53] M. Prioux, S. Duluard, F. Ansart, G. Pujol, P. Gomez, L. Pin, Advances in the control of electrophoretic process parameters to tune the ytterbium disilicate coatings microstructure, J. Am. Ceram. Soc. 103 (12) (2020) 6724–6735, https://doi.org/10.1111/jace.17365.